Aquatic Botany 196 (2025) 103821

Contents lists available at ScienceDirect

Aquatic Botany

journal homepage: www.elsevier.com/locate/aquabot

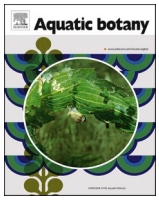

Carbon allocation dynamics of *Spartina alterniflora* in Georgia saltmarsh, USA

Yeajin Jung [1,*], Adrian Burd

Department of Marine Sciences, University of Georgia, Athens 30605, USA

ARTICLE INFO

Keywords:
Saltmarsh production model
Carbon translocation
Blue carbon

ABSTRACT

We developed a phenology-based growth model(PG model) for *Spartina alterniflora* that incorporates the effects of light, temperature, and salinity on plant production. The PG model is the first to quantify carbon translocation between both above- and below-ground biomass across three phenological periods: growth, senescence, and dormancy periods. This model, fitted to field data from short, medium, and tall *S. alterniflora* types, estimates physiological parameters such as mass-specific rates of carbon translocation. Once parameterized, the model is applied in forward mode to predict whole-plant production, growth, respiration, mortality, and translocation. Model results reveals that short forms allocate 82 % of photosynthate to below-ground biomass during the growing season, compared to tall (52 %) and medium (22 %) types. However, tall forms, with extensive above-ground biomass, show the highest absolute carbon translocation to below-ground tissues during growth(ave. 3940 g dry weight m^{-2}) and senescence(ave. 265 g dry weight m^{-2}) period. An average mortality rate of 52 % of net production in the tall form below-ground biomass throughout the year indicates a substantial contribution to organic carbon sequestration within the habitat sediment. Model results also reveal that the carbon translocation from below- to above-ground tissues may not be required for survival during winter in milder climate like Sapelo Island, Georgia.

1. Introduction

Salt marshes are vital coastal ecosystems that provide numerous ecosystem services, including habitat provision, coastal protection, water filtration, and carbon sequestration (Whitfield, 2017; Shepard et al., 2011; Townend et al., 2011). The production and accumulation of biomass in salt marshes are key to their role as significant carbon sinks, with the potential to sequester carbon at rates over 30 times higher than tropical forests (Mcleod et al., 2011; Davis et al., 2015). *Spartina alterniflora*, a dominant C4 deciduous halophyte, is the most prevalent and productive salt marsh grass along the U.S. East Coast (Dawes, 1998; O'Donnell and Schalles 2016). It exhibits three distinct growth forms, each contributing significantly to blue carbon sequestration.

The tallest form, exceeding 1 m, thrives near creek banks in soils with relatively low porewater salinity, while the shortest form, less than 50 cm, occupies the marsh interior where salinities are higher (Anderson and Treshow, 1980). The medium height form is found in areas with intermediate salinity levels. Notably, *S. alterniflora*'s above-ground production ranges from 0.4 to 2.2 kg m^{-2} y^{-1}, but its below-ground production is generally more substantial, varying between 3.5 and 3.9 kg m^{-2} y^{-1}, and can even reach up to 7.4 kg m^{-2} y^{-1} in marshes along the northern Gulf of Mexico (Stagg et al., 2017). However, most production studies have predominantly focused on above-ground dynamics, thus overlooking the critical aspects of below-ground production, storage, and the timing of resource translocation (Gallagher et al., 1980; Howes et al., 1986; Więski and Pennings, 2014).

Regional differences in *S. alterniflora* productivity are largely attributed to geographical variations in climate, salinity, and phenology (Seneca and Broome, 1972; Seneca and Blum, 1984). Field experiments have shown a negative correlation between *S. alterniflora* biomass and salinity (Drake and Gallagher, 1984; Nestler, 1977). Richards et al. (2005) demonstrated that as salinity increases, the number of leaves of salt marsh grasses rises while their leaf sizes diminish, impacting their above-ground biomass. Importantly, the timing and duration of resource translocation between above- and below-ground tissues are linked to other events in the plant's life cycle. For instance, *S. alterniflora* begins allocating carbon to below-ground tissues with the onset of flowering (Crosby et al., 2015), and an increase in rhizome biomass coincides with

* Corresponding author.
E-mail address: yjjung@kmi.re.kr (Y. Jung).
[1] Marine Research Division, Korea Maritime Institute, Busan 49111, South Korea (Permanent address)

https://doi.org/10.1016/j.aquabot.2024.103821
Received 12 May 2024; Received in revised form 9 September 2024; Accepted 12 September 2024
Available online 13 September 2024

foliage senescence (Elsey-Quirk et al., 2011). These phenological characteristics may determine the amount of material a plant can store in below-ground tissues during winter. This in turn, affects the resources available for growth in the early spring of the following year and the amount of inorganic carbon sequestered in soils. Despite their importance, these sub-annual dynamics are frequently overlooked in growth dynamic models.

According to the isotope study by Peterson and Howarth (1987), the origin of organic matter in Sapelo Island was identified as *Spartina* and algae, with no detection of terrestrial sources. Recent findings by Craft (2023) indicate that the organic carbon content in the sediment of *Spartina* habitats on Sapelo Island is about 5–6 %, with carbon sequestration rates of 75–85 g C m^{-2} yr^{-1} in natural wetlands and 118–125 g C m^{-2} yr^{-1} in restored salt marshes. This information highlights the significance of autochthonous below-ground carbon storage and the role of sediment in the overall carbon sequestration potential of these ecosystems.

A limited number of models exist for the growth and production of *S. alterniflora*, with even fewer addressing both above- and below-ground processes (Morris et al., 1984; Cunha et al., 2005; Zheng et al., 2016). Models by Morris et al. (1984) and Dai and Wiegert (1996) were among the first to estimate *S. alterniflora*'s annual below-ground production rates, revealing that ignoring carbon translocation between above- and below-ground tissues could significantly overestimate net production estimates. However, these models considered translocation in a unidirectional manner, solely from above-ground to below-ground tissues. A recent model for *S. alterniflora*, proposed by Zheng et al. (2016), incorporates phenological aspects and bidirectional translocation of biomass. Adapted from models originally designed for *Typha* species and *Phragmites australis* (Asaeda and Karunaratne, 2000; Asaeda et al., 2005), the *S. alterniflora* model utilized literature data, covering a wide geographic range from the U.S. East Coast to China, and highlighted geographic variations in root-to-shoot ratios. Yet, it required difficult-to-acquire data, such as mortality and respiration rates of 1-year-old rhizomes.

In our study, we present the Phenology-based Growth Dynamics model (PG model) for *S. alterniflora*, developed from field data across different growth forms in Georgia, USA. Our model integrates key aspects from Morris et al. (1984) and Zheng et al. (2016) and expands upon these by considering the impact of salinity on plant production across three phenological stages: growth, senescence, and dormancy. This comprehensive approach provides novel insights into the dynamics of biomass translocation within *S. alterniflora*.

Our research questions are: (1) Does the PG model effectively describe the allocation patterns of above- and below-ground biomass of the short, medium, and tall forms of *S. alterniflora*? (2) How do translocation rates and the amount of translocated material differ for the three types of *S. alterniflora* during growth, senescence, and dormancy?

We hypothesize that for *S. alterniflora* in Georgia: (1) the short form of *S. alterniflora* will show a greater transfer of photosynthates to below-ground tissues compared to the medium and tall forms, reflecting a higher root:shoot ratio. (2) the below-ground assimilate translocation to above-ground tissue occurs in all three forms of *S. alterniflora* during early spring to counteract the limited radiation and low temperature that constrain growth.

2. Methods and materials

2.1. Site location

Plants were collected close to 18 permanent plots, 6 for each height form of *S. alterniflora,* located in monotypic areas of tall, medium, and short form *S. alterniflora* on Sapelo Island, Georgia, on the southeastern coast of the USA (Fig. 1). Samples of the tall, medium, and short forms of *S. alterniflora* were respectively collected from creekbank, intermediate areas between creekbank and high marsh, and high marsh locations. The high marsh regions typically experience less frequent inundation than creekbank areas, leading to higher porewater salinity and increased sulfide concentration. The plots are located within the domain of the Georgia Coastal Ecosystem Long Term Ecological Research (GCE-LTER) program, and close to the Duplin River and adjacent to the GCE-LTER flux tower (31°26′37.6″ N, −81°17′1.9″ W). Irradiance data was taken from the climate monitoring station at Marsh Landing (31°25′4.2″ N, −81°17′43.5″ W), less than 4 km from the plots.

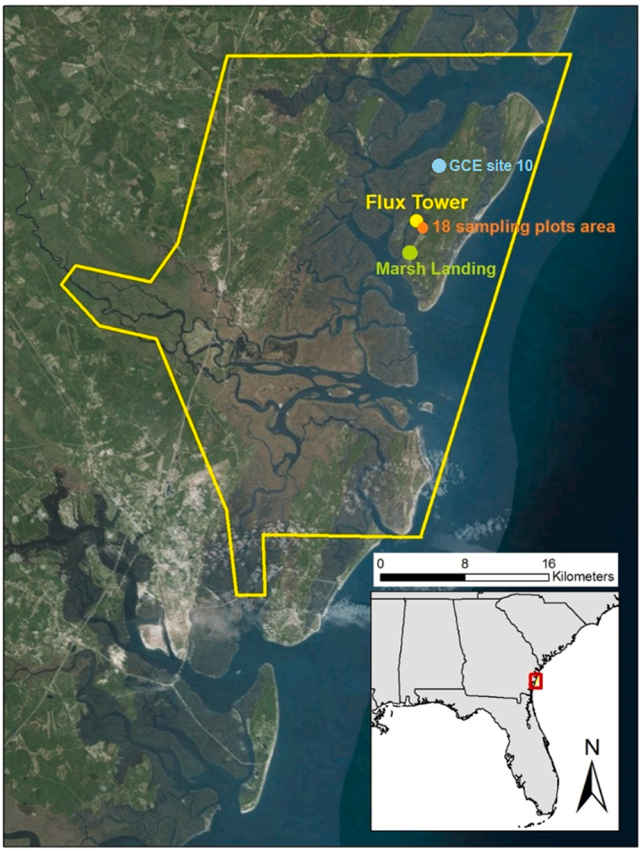

Fig. 1. Site map showing the location and boundary of the Georgia Coastal Ecosystem Long Term Ecological Research (GCE-LTER) site on Sapelo Island (Georgia, USA), the location of the flux tower, the Marsh Landing weather station, GCE site 10, and the area of the 18 sampling plots where the destructive core samples were collected.

2.2. Sampling and biomass estimation

Destructive core sampling was conducted monthly from October 2013 to December 2014, targeting 6 tall, 6 medium, and 6 short *S. alterniflora* permanent plots adjacent to the GCE flux tower. Above-ground tissues were harvested at the ground level, while below-ground tissues were extracted using a PVC pipe of 7.5 cm diameter, inserted into the sediment to a depth of 30 cm. The harvested samples were refrigerated at 4 °C overnight and subsequently washed over an 800 μm sieve the following day to separate living roots and rhizomes from soil particles. The samples obtained from the destructive core sampling were oven-dried at 60 °C for three days, then weighed to

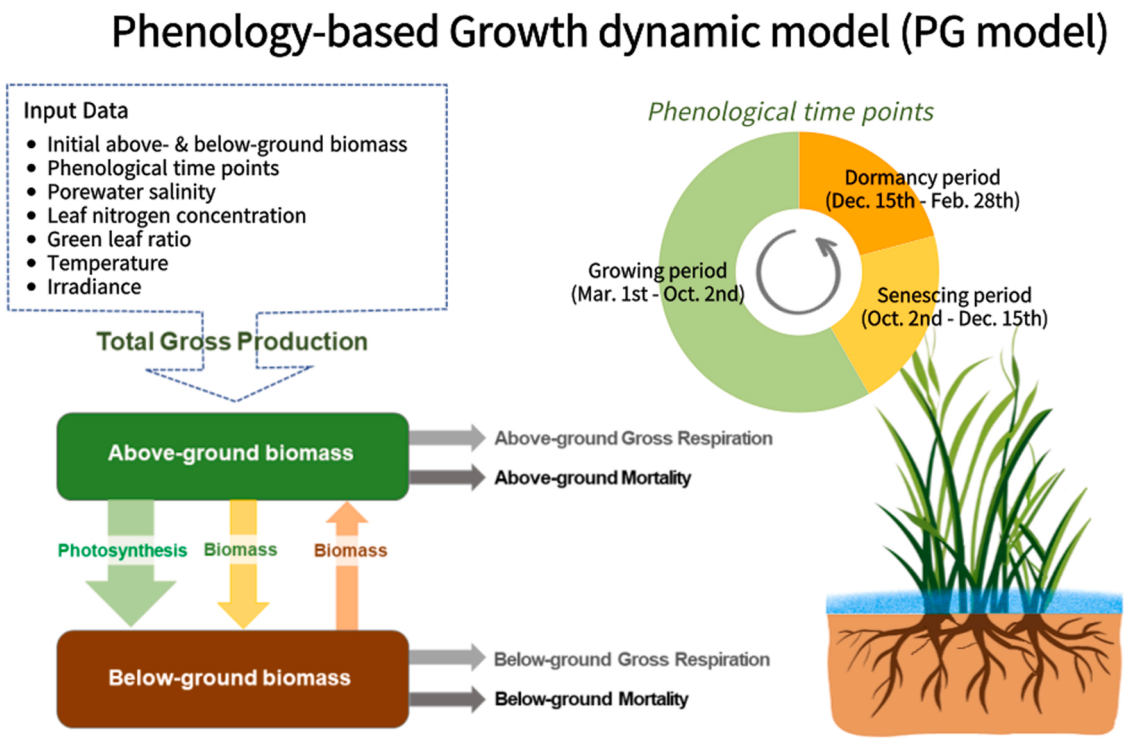

Fig. 2. Structure of the *S. alterniflora* phenology-based growth dynamic model (PG model) adapted from Morris et al. (1984) and Zheng et al. (2016)).

calculate the aboveground biomass-to-belowground biomass ratios. Concurrently, plant height data were collected at the same site and during the same period using non-destructive methods. This involved measuring the height of all shoots exceeding 10 cm. Shoots below 10 cm were not measured due to their minimal contribution to total above-ground biomass, allowing us to minimize the effort within the limited time for data collection. In the case of short and medium *S. alterniflora*, this involved using a 0.25 m x 0.25 m quadrat in the center of each plot, and a 0.5 m x 0.5 m quadrat for the tall form *S. alterniflora*. The shoot-to-root ratios, combined with the plant height data, facilitated the extrapolation of biomass calculations to a per square meter area (Fig. 3 and Table A.1). These calculations were based on allometric equations adapted from Pennings (2002) for the GCE site 10, adjacent to our study site. The allometric equation for the tall form *S. alterniflora* growing on the creek bank is as follows:

$$Aboveground\ biomass(g) = \exp(-6.11 + 1.75\log(plant\ height(cm))) \quad (1)$$

The allometric equation used for *S. alterniflora* growing in the mid-marsh is:

$$Aboveground\ biomass(g) = \exp(-7.31 + 1.99\log(plant\ height(cm))) \quad (2)$$

This equation was applied to both medium and short forms of *S. alterniflora*. The below-ground biomass was estimated from above-ground biomass using the root-to-shoot ratio from core samples, applied when direct field data was unavailable. Given that only live below-ground biomass was measured in the cores, the model is designed to estimate live below-ground biomass. The data collected from this study is accessible via the GCE-LTER website at https://gce-lter.marsci.uga.edu/public/data/data.htm.

2.3. Modeling S. alternilflora growth dynamics

We introduced the Phenology-based Growth dynamics model, a novel construct that integrates salinity impacts, air temperature, and irradiance data into the biomass production and translocation analysis. This model allowed for an in-depth understanding of the carbon allocation within *S. alterniflora* across various phenological stages.

2.3.1. Environmental and biological parameter measurement

The model also incorporates air temperature and irradiance data (Fig.A.2). Hourly air temperature measurements were sourced from the GCE Flux Tower, a level 3 weather station that records environmental data at three different elevations, situated near the sampling site. Additionally, hourly downwelling irradiance data were acquired from the Marsh Landing weather station, located less than 4 km from the GCE Flux Tower.

Our production model addresses the seasonal variability in the green, photosynthetically active fraction of the *S. alterniflora* canopy by incorporating two key biotic variables: the green fraction (F) of the canopy, defined as the ratio of green leaf and stem biomass to total canopy biomass, and the percent nitrogen content in green leaves, following Morris et al. (1984). Canopy data for F, sourced from tall *S. alterniflora* specimens collected between 2013 and 2014 (Jung and Burd, 2017), was applied to all plants in the model. Additionally, the model includes monthly nitrogen content data for these plants from Sapelo Island, as reported by Morris et al. (1984).

2.3.2. Influence of porewater salinity on S. alterniflora biomass production

Within this model, both the gross production (G) and respiration rates (R) are estimated based on the methodology outlined in Morris et al. (1984). Gross production is determined by several factors

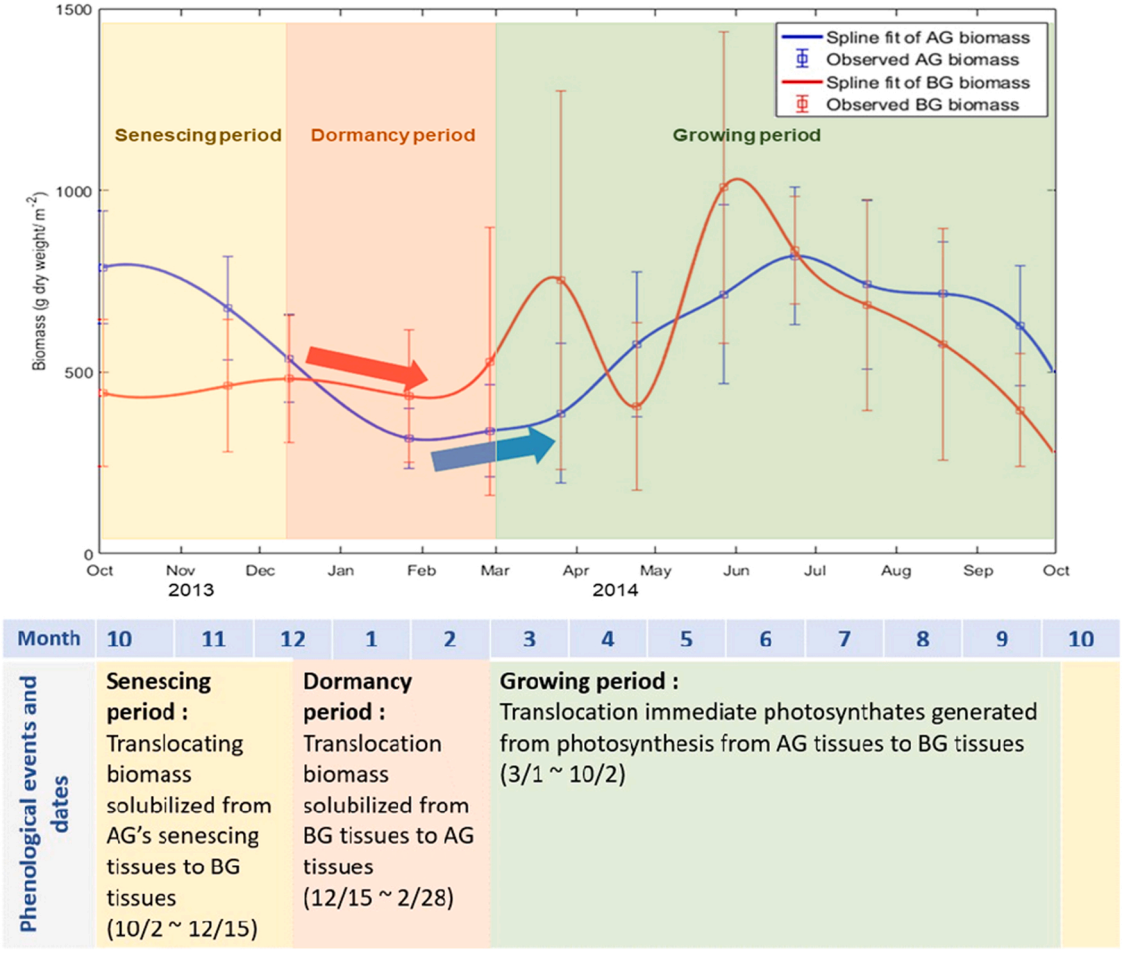

Fig. 3. Three phenological events and dates based on monthly average above-ground (AG) and below-ground (BG) biomass field data (with standard deviations) from Oct. 2013– Dec. 2014 in tall form *S. alterniflora* on Sapelo Island, Georgia, USA.

Table 1
Definitions of symbols and parameter values.

Symbol	Definition	Units & Value
P	Total net production	g dry wt m^{-2} h^{-1}
B_c	Sum of above and below-ground biomass	g dry wt m^{-2}
B_{above}	Above ground biomass	g dry wt m^{-2}
B_{below}	Below ground biomass	g dry wt m^{-2}
T	Air temperature	°C
ϑ	Solar elevation	Radians
L	Solar irradiance at the canopy apex	W m^{-2}
λ	Irradiance at half-max photosynthesis	300 ± 100 W m^{-2}
α	Irradiance extinction rate within the canopy	$(3.4 \pm 1.0)\times10^{-4}$ m^2 $gdwt^{-1}$
N	Nitrogen percentage of dried leaves biomass	%
F	Quotient of green leaf weight: total canopy weight	Dimensionless
ψ	Temperature coefficient for gross production	$(7.1 \pm 1.7)\times10^{-4}$ $°C^{-1}$ h^{-1}
η	Nitrogen concentration at half-max growth	0.36 ± 0.29 % dwt
ρ	Temperature coefficient for dark respiration	$(2.3 \pm 0.6)\times10^{-5}$ $°C^{-1}$ h^{-1}

including total canopy biomass, air temperature, canopy-top irradiance, solar elevation, the ratio of green leaves, and leaf nitrogen content. The rates of above- and below-ground respiration were derived as functions of temperature, the ratio of green leaves, and biomass (see Eq. 3). Total net production before applying the salinity effect, *Pinit*, was calculated as follows:

$$Pinit = \frac{\psi TNF\sin(\vartheta)\left\{\ln\left(Le^{\frac{\alpha B_c}{\sin(\vartheta)}}+\lambda\right)-\ln(L+\lambda)\right\}}{(\alpha(N+\eta))} - \rho T(FB_{above}+B_{below}) \quad (3)$$

← Gross production (G) → ← Respiration (R) →

where Table 1 provides the symbols and values for the constants.

The net production after applying the salinity effect, P, was as follows.

$$P = 10^{-5}G^3 - 0.0011G^2 + 0.0042G - 1.1855 - R \quad (4)$$

To incorporate the impact of salinity on production and consequently the height of *S. alterniflora*, we developed a salinity-dependent equation

that multiplies gross production (Eq. 4). Eq. (3) and its associated parameter values were derived from *S. alterniflora* cultures under different shading and nitrogen levels (Morris 1982); the average salinity of the water in these cultures was approximately 17.5 ppt. To incorporate the effects of variable salinity on production, we devised a parameterization of the effects of salinity on the gross production rate for *S. alterniflora* (Eq. 4). It is based on empirical evidence from studies investigating the relationship between salinity and production (Linthurst and Seneca, 1981; Ge et al., 2014; Medeiros et al., 2013; Howes et al., 1986).

Our approach results in a factor that adjusts the gross production, set to 1 in conditions with a salinity of 17.5 ppt. *S. alterniflora* tolerates regular inundations within a salinity range of 0–35 ppt and do not usually inhabit areas with salinity levels above 45 ppt (Medeiros et al., 2013; Howes et al., 1986). The 60ppt represent bare patch areas where no vegetation is found. In the development of these parameters, we posited that gross production halts at salinities exceeding 45 ppt, a dynamic accurately depicted by Eq. 4.

Eq. (3) lacks an explicit representation of translocation between above- and below-ground tissue and mortality. To address this limitation and integrate these processes, we incorporated formulations for mortality and biomass translocation between above- and below-ground tissues from the model developed by Zheng et al. (2016). Equations for the above- and below-ground biomass were formulated to reflect a balance among production, mortality losses, respiration, and translocation.

$$\frac{dB_{above}}{dt} = G - R_{above} - M_{above} - TB_{above_{to_{below}}} + TB_{below_{to_{above}}} - TP_{above\_to\_below} \quad (5)$$

$$\frac{dB_{below}}{dt} = TB_{above\_to\_below} + TP_{above\_to\_below} - TB_{below\_to\_above} - R_{below} - M_{below} \quad (6)$$

In these equations, B, G, and R signify biomass, gross production, and respiration rate, respectively. TB, TP, and M represent carbon translocation, photosynthate translocation, and mortality rates between above- and below-ground biomass.

Forward model simulations were conducted by solving Eqs. (5) and (6), which account for above- and below-ground biomass. These simulations utilized translocation and mortality parameter values corresponding to the salinity ranges of regions where short, medium, and tall forms of *S. alterniflora* were observed. To solve these equations, we employed a 4th order Runge-Kutta method (Press et al., 2002), with a constant time step of one hour. All computer codes for our study were developed and executed using Matlab 2016b. The forward simulations spanned from October 2013 to December 2015, a timeframe that extends beyond the period utilized for model parameterization. We then compared the model results with the observed above- and below-ground biomass data corresponding to this extended period. The differences between observed and modeled biomass, ΔD_i, were normalized to the standard deviation of the filed estimates.

The daily mortality rate was computed as a function of temperature and biomass, following the approach by Zheng et al., (2016).

$$M_{above} = m_a \theta^{(T-20)} B_{above} \quad (7)$$

$$M_{below} = m_b \theta^{(T-20)} B_{below} \quad (8)$$

In the equation that describes mortality rate, the symbol θ is used for the temperature constant, assigned a value of 1.09. The parameters, m_a and m_b, represent the specific mortality rates for above-ground and below-ground tissues at 20°C, respectively, for different height forms *of S. alterniflora* on Sapelo Island. These rates were determined using the PG model in its inverse mode (Table 2). The inverse mode approach (Soetaert and Petzoldt, 2010) is employed to determine unknown parameter values that align closely with observed biomass data and to serve as a forward model for predicting daily production and biomass translocation over the course of a year.

2.3.3. Carbon allocation dynamics

The bidirectional carbon translocation rates were determined using the equations specified in Zheng et al. (2016).

$$TP_{above\_to\_below} = \alpha_{ab} G \quad (9)$$

$$TB_{above\_to\_below} = \gamma B_{above} \quad (10)$$

$$TB_{below\_to\_above} = \alpha_{ba} \theta^{(T-20)} B_{below} \quad (11)$$

where $TP_{above\_to\_below}$ is the translocation rate of photosynthates from above- to below-ground tissues during growing period, $TB_{above\_to\_below}$ refer to the rate of assimilates translocation from above- to below-ground tissues during plant senescence, and $TB_{below\_to\_above}$ denotes the rate of assimilate translocation from below- to above-ground during the dormancy period. The symbols definitions and parameter values in Eqs. 9 – 11 are given in Table 2.

2.3.4. Phenological phases

We incorporated the local phenological dates specific to our study site (Fig. 3). These dates are expressed numerically as the day-of-year, with January 1st designated as day 1. In our model, we define the dormancy period as the period during which the below-ground tissues remobilize assimilates and translocate soluble carbon to the above-ground biomass to support above-ground survival during the winter and growth in early spring. This period is also when plants are not actively growing, even though there may be sufficient irradiance to support photosynthesis.

In the PG model, major phenological events are mapped to specific day-of-year numbers, where January 1st is day 1. The dormancy period's assimilate translocation from below-ground to above-ground

Table 2
Symbol definitions and parameter values from the inverse model (Oct. 2013–Dec. 2014) and total ΔD_i (sum of ΔDa_i and ΔDb_i)calculation using the PG model (Oct. 2013–Dec. 2015). The value less than 10^{-7} is denoted as 0.

Symbol (unit)	Definition	Tall form *S. alterniflora*	Medium form *S. alterniflora*	Short form *S. alterniflora*
α_{AB} (fraction)	Proportion of photosynthate allocated to below-ground tissues during growth	0.52	0.22	0.82
α_{BA} (fraction)	Proportion of below-ground assimilate allocated to above-ground tissues during dormancy	0	0	0
γ (fraction)	Proportion of above-ground assimilate allocated to below-ground tissues during senescence	0.0008	0	0.0013
m_a (gg^{-1} d^{-1})	Specific rate of above-ground mortality at 20 °C	0.0006	0.0012	0
m_b (gg^{-1} d^{-1})	Specific rate of below-ground mortality at 20 °C	0.0005	0	0.0002
Total ΔD_i	Sum of the differences between observed and modeled biomass	72.69	77.07	57.64

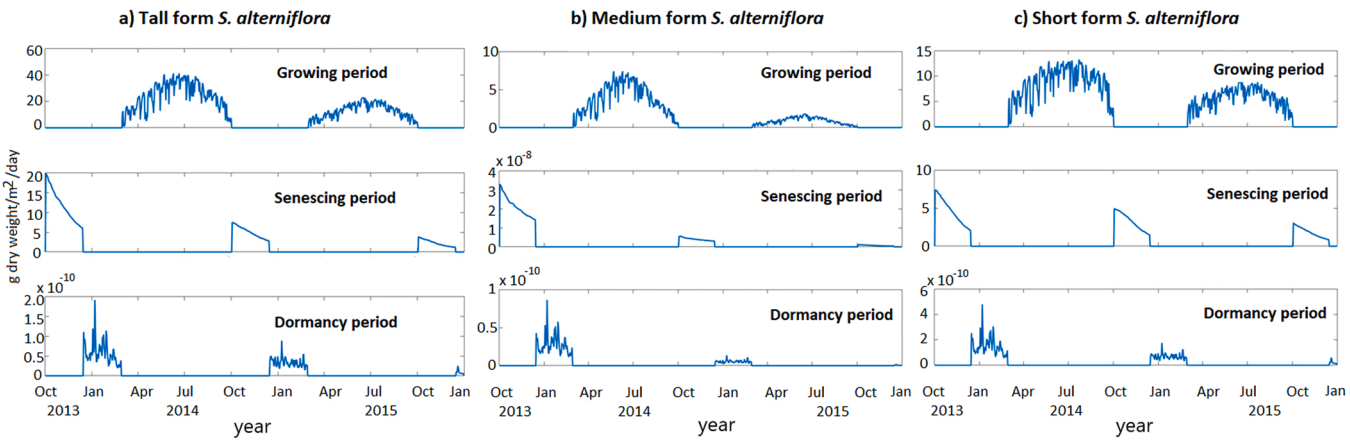

Fig. 4. Modeled daily carbon translocation from AG to BG during growing & senescing period, and from BG to AG during dormancy period for tall(a), medium(b), short(c) form *S. alterniflora* on Sapelo Island, Georgia.

tissues initiates on December 15th, marked as SBbelow_to_above, with a value of 349. This translocation concludes on February 28th (EBbelow_to_above: 59), marking the end of the dormancy period's below-ground to above-ground assimilate movement.

The growing season sees the start of photosynthate translocation from above-ground to below-ground tissues on March 1st, identified as SPabove_to_below, with a value of 60. This process ends on October 2nd (EPabove_to_below: 275), also signaling the beginning of assimilate remobilization and translocation from senescing above-ground to below-ground tissues for the senescence period. The phenological dates for the tall form of *S. alterniflora* were estimated by identifying the onset of senescence in the collected above-ground biomass and analyzing the seasonal patterns of both above- and below-ground biomass (Fig. 3). A cubic spline was utilized to interpolate between the data points. We chose the sampling date of 2nd October when we first observed yellow senescing shoot biomass of more than 10 g core^{-1} as the date of onset of senescence ($EP_{above\_to\_below}$). From the date of the start of senescence, we assume that *S. alterniflora* starts to remobilize assimilate from senescing tissues and translocate soluble carbon to the below-ground biomass to store the energy in the root and rhizome. A steady decrease in below-ground biomass was observed from December to the end of February (Fig. 3 & Table A.1), and we defined this phase as the dormancy period. Upon the end of the dormancy period, when environmental conditions become favorable for active growth, plants commence an increase in above-ground biomass. This phenological phase is designated as $SP_{above\_to\_below}$. The interval from $SP_{above\_to\_below}$ to the onset of senescence ($EP_{above\_to\_below}$) is referred to as the growing period.

Given that our study sites for tall, medium, and short *S. alterniflora* are within a 5000 m^2 area and the Phenocam, which captures images of the salt marshes near our site every 30 minutes, couldn't differentiate the zonation of *S. alterniflora* forms, we applied the same phenological dates to all three forms.

2.3.5. Determining PG model parameters

To ascertain the parameter values utilized in the PG model (Table A.2), we employed the model in inverse mode. This approach enabled us to identify the parameter values that most closely aligned with the observed biomasses from October 2013 to December 2014. This was achieved by minimizing the cost function.:

$$\chi^2 = \sum_{i=t_s}^{t_e} \frac{\left((FA_i - MA_i)^2 + (FB_i - MB_i)^2\right)}{{\sigma_i}^2} \quad (12)$$

where, t_s represents the date of the first observation and t_e denotes the time of the last observation. *FA* and *FB* represent field measurements at *i*-th time point for above- and below-ground biomass, respectively. The *FA* biomass was determined using an allometry equation that relates biomass to plant height(cm) (Pennings, 2002). The plant height surpassing 10 cm was recorded at the center of each plot within the quadrat. The field below-ground biomass (*FB*) was calculated by multiplying the field above-ground biomass (*FA*) by the root-to-shoot ratio derived from the monthly destructive core samples. *MA* and *MB* refer to the above- and below-ground biomass predicted by the PG model at *i*-th time point. Fmincon, a constrained nonlinear minimization routine in Matlab that employs an interior point algorithm, was used to minimize the cost function.

3. Results

3.1. Carbon allocation dynamics at different phenological periods

The fractions of the photosynthate translocated from above- to below-ground (α_{ab}) tissues in tall, medium, and short form *S. alterniflora* were 0.52, 0.22, and 0.82, respectively (Table 2).

However, the amount of photosynthate (g m^{-2}) translocated from above- to below-ground tissues throughout the whole growth period was highest in tall form *S. alterniflora* (Table A.2 & Fig. 4) and was approximately 3 – 6 times that of the other height forms.

The fraction of above-ground carbon translocated from above- to below-ground tissues during senescence (ɣ) was higher in short form *S. alterniflora* (0.0013) compared to tall and medium form *S. alterniflora*, which had effectively zero translocation rates, respectively (Table 2). However, the absolute biomass translocated from above- to below-ground during the whole senescence period was greater in tall form *S. alterniflora* (Table A.2).

The proportion of below-ground assimilate allocated to above-ground tissues during dormancy (α_{BA}) is almost zero in all types of *S. alterniflora*. This 0 value of α_{BA} suggest that *S. alterniflora* on Sapelo Island do not translocate stored resources from below- to above-ground

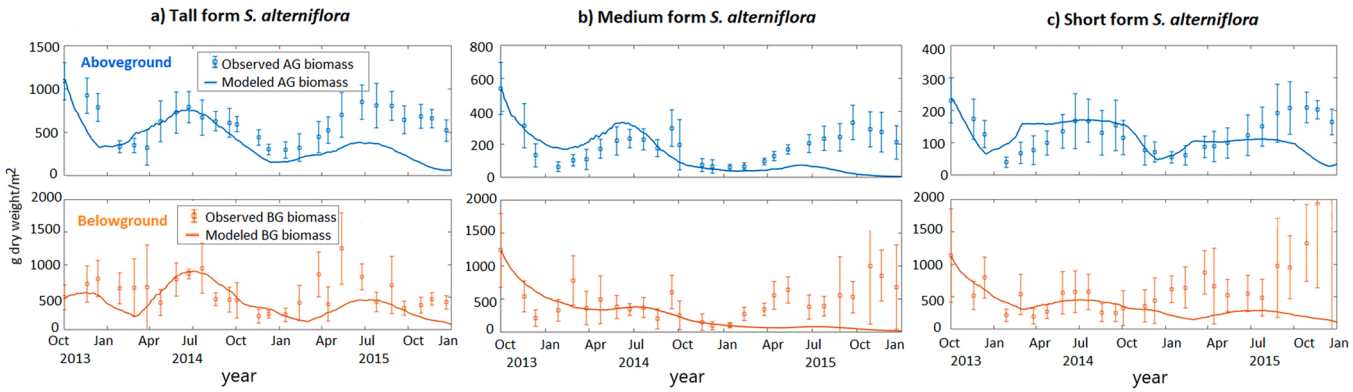

Fig. 5. The PG model result of tall(a), medium(b), short(c) form *S. alterniflora* on Sapelo Island, Georgia.

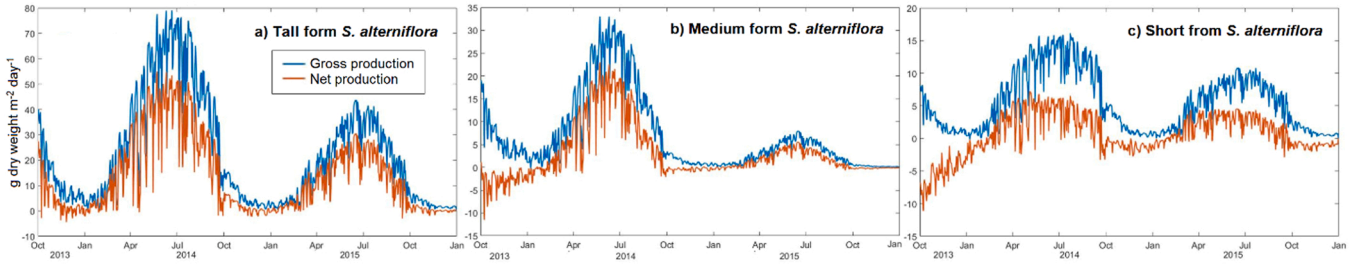

Fig. 6. Gross production and net production of the three types of *S. alterniflora* on Sapelo Island, Georgia.

tissues during the winter.

The specific rate of above-ground mortality at 20°C (parameter m_a) were 0.0006 and 0.0012 gg^{-1} d^{-1} in tall and medium form *S. alterniflora,* respectively but essentially zero in short form *S. alterniflora.* The specific rate of below-ground mortality at 20°C was similar for tall and short height forms but almost zero in medium form *S. alterniflora* (Table 2).

We estimated total carbon translocation during growth, senescence, and dormancy periods using the PG model. Assimilate translocation from below-ground to above-ground tissues was minimal (close to zero) during the dormancy seasons in all types of *S. alterniflora* (Fig. A.1). Translocation of the remobilization of assimilate from above-ground tissues during senescence in tall *S. alterniflora* was 1.5 folds that in short height forms in 2014 and similar in 2015 (Table A.2 & Fig. 4). During the growing season, tall *S. alterniflora* translocated approximately 24 g d^{-1} during summer 2014 compared to 4 g d^{-1} for medium and 9 g d^{-1} for short *S. alterniflora* in 2015.

3.2. Biomass prediction

The model was fitted to the observed biomass from Oct. 2013 to Dec. 2014 for estimating parameters. In the following year 2015, both above- and below-ground biomass was predicted by the model using the calculated parameters. The PG model underestimated above-ground biomass (AG) of tall *S. alterniflora* during the last year (2015) of the study (Fig. 5a). A similar pattern was observed in the model results for medium *S. alterniflora* (Fig. 5b), and from the fall seasons for the short form (Fig. 5c). The model predicted the general pattern of below-ground biomass of tall *S. alterniflora* whereas it underestimated the below-ground biomass in other two height forms (Fig. 5).

Overall, the model predicted the above- and below-ground biomass of short form *S. alterniflora* best based on its lowest total ΔD_ivalues (Table 2 & Fig.A.1).

The general patterns of the gross and net production (Fig. 6) of the three height forms of *S. alterniflora* closely followed seasonal irradiance and temperature cycles (Fig.A.2).

Both gross and net production were highest in the tall form *S. alterniflora*, followed by the medium and short *S. alterniflora* (Fig. 6). The gross production was approximately five times higher in tall *S. alterniflora* than in short *S. alterniflora* during the active growing season between late spring (April) and late summer (August). The net productions of medium and short *S. alterniflora* had negative values in the first winter of the study period, which indicates that there was more consumption from respiration than production from photosynthesis. During this period, the gross production dropped rapidly and stayed near zero.

Mortality rates in *S. alterniflora* varied seasonally across the three types, with the highest in tall, then medium, and lowest in short forms. Tall and medium forms had similar mortality rates for both tissue types (4.85–7.83 g m^{-2} d^{-1}). In contrast, the short form showed an almost negligible above-ground mortality, while its average daily below-ground mortality was the lowest among the three types, at approximately 2 g m^{-2} d^{-1} (Table A.3). For all three *S. alterniflora* types, below-ground respiration rates were higher than above-ground biomass, with the tallest form respiring the most(4.97 g m^{-2} d^{-1}). In the short form,

below-ground respiration(3.82 g m^{-2} d^{-1}) was about four times that of above-ground(1.02 g m^{-2} d^{-1}). All *S. alterniflora* types exhibit their highest respiration rates in the summer, correlating with higher temperatures. Above-ground respiration falls to less than 8 g m^{-2} d^{-1} in early spring (Fig.A.3).

3.3. Sensitivity analyses of phenological dates

Sensitivity analyses were conducted on the PG model's phenological dates to evaluate the relative significance of phenological date variations on biomass predictions (Table A.4). We compiled four sets of each baseline date by varying between ± 10 and ± 20 days and compared the dates in this study to the dates estimated from the Phenocam data (O'Connell, pers. comm.). The model results were most sensitive to changes in the start date of assimilate translocation from below- to above-ground tissues, particularly in the above-ground biomass. The differences between our date and O'Connell's date was 5 days, which changed the above-ground biomass by about 19 % and the below-ground biomass by approximately 4 % from our modeled biomass.

4. Discussion

This study aimed to enhance our understanding of *S. alterniflora*'s growth and carbon allocation dynamics by developing a Phenology-based Growth Dynamic Model. We achieved advancements by incorporating the effects of salinity on growth and quantifying carbon translocation between above- and below-ground tissues across three phenological periods: growth, senescence, and dormancy. This work contributes to our knowledge of carbon dynamics in this crucial blue carbon species.

4.1. Comparative analysis of biomass translocation

Our initial hypothesis posited that the short form of *S. alterniflora* would translocate a larger proportion of its above-ground assimilates and photosynthates to below-ground tissues compared to other forms. Although the translocation parameters α_{ab} and γ (Eqs. 9 – 11) indicated a higher rate in the short form (Table 2), the total volume of material translocated was actually greatest in the tall form (Table A.2), likely due to its larger above-ground biomass.

The increased carbon allocation to below-ground tissues in the short form of *S. alterniflora* over the tall form, likely acts as an adaptive mechanism to the challenging soil conditions encountered in high marsh environments. In our research, samples of the tall form were obtained from creekbank locales, while the short form was gathered from high marsh areas. Typically, marsh interiors experience less frequent inundation compared to creekbank locations, resulting in elevated porewater salinity (Redfield, 1972; Smart, 1986; Gross et al., 1991; Miklesh and Meile, 2018) and increased soil sulfide concentrations (King et al., 1982). Such heightened porewater salinity necessitates greater energy expenditure for osmotic regulation (Hessini et al., 2009). Furthermore, elevated sulfide levels introduce additional stressors, including a more adverse redox potential due to available free sulfide electrons and sulfide toxicity, prompting a strategic shift in resource allocation towards below-ground tissues by the plants.

The *Spartina* biomass computed by Zheng et al. (2016)'s model exhibited a fluctuation pattern similar to our model. In particular, we noted that the peak of below-ground biomass tends to follow the pattern of the above-ground biomass with a lag of approximately two months. Zheng et al.(2016) extrapolated above-ground data collected in Georgia, USA. from Dai and Wigert (1996) and calculated below-ground data, whereas we use direct measurements of both above- and below-ground biomass in the PG model. While differences in methodology and data sourcing pose challenges for direct comparison, the convergence in fluctuation patterns between the two models suggests intriguing underlying biological processes worth further exploration.

Furthermore, the differences between our phenological dates and those proposed by O'Connell were less than 8 days, except for a notable 21-day discrepancy regarding the start date for assimilate translocation from senescing above-ground tissues to below-ground tissues. Considering our monthly sampling regime and the initial detection of dominant senescing biomass in October samples, we designated the first instance of senescing tissues exceeding 10 g per core as the threshold for marking the start of photosynthate translocation and senescence initiation. The variance in biomass estimates between our findings and O'Connell's, which was less than 26 %, validates our methodology for determining phenological dates by examining the patterns of dead and living biomass. This technique could be especially useful in areas without access to Phenocam data.

4.2. Limited winter biomass translocation in Southern S. alterniflora

The second hypothesis, that *S. alterniflora* in Georgia translocates biomass from below- to above-ground biomass during dormancy, is not supported by our results. Translocated assimilates from below- to above-ground tissues during dormancy period are close to zero in all types of *S. alterniflora* (Table A.2). Geiger (1969) demonstrated that C3 plants of *Cirsium arvense* from Montana have a higher translocation rate than those from California at a lower temperature. In Potvin et al., (1984), C4 grass from Quebec showed more active sinks than those from Mississippi. The low translocation rates from below- to above-ground during plant dormancy could be because the photosynthesis in *S. alterniflora* on Sapelo Island is sufficient to support the above-ground biomass, even during the winter. Consequently, the above-ground components may not serve as active sinks, which in turn decreases translocation from below- to above-ground. Another possible reason for the low translocation rate is that the stored carbon in below-ground tissues might be used to support the survival of below-ground tissues, thereby limiting the availability of biomass to translocate from below to above-ground tissues. Translocating the carbon from above- to below-ground takes energy in terms of remobilization of assimilates and transporting the soluble carbon to root and rhizomes. Supplying carbon to above-ground tissues through photosynthesis and utilizing remobilized carbon from roots and rhizomes for below-ground tissues could be more energy-efficient. This approach minimizes energy consumption by allocating carbon during seasons unfavorable for plant growth and development. However, the model results do suggest the possibility that the internal dynamics of resource allocation and translocation may differ with the location of plants in the marsh. This indicates the necessity for additional research, integrating field studies, greenhouse experiments, and model enhancement, particularly considering the critical role of below-ground storage and biomass at the close of one growing season in influencing plant production in the subsequent year.

Additionally, examining mortality trends in both above- and below-ground biomass offers insights into the portion of biomass that could be sequestered in sediment layers. The limited carbon translocation from belowground to aboveground biomass, combined with the significant average mortality rate of approximately 52 % of net production in the belowground biomass of tall-form *S. alterniflora*, supports the idea that tall-form *S. alterniflora* plays a crucial role in the burial of organic carbon

within its native soils. This finding highlights its function as an important sink for blue carbon.

4.3. Model needs and limitation

The PG model tends to underestimate the above-ground biomass of tall and medium *S. alterniflora* during the final year of our study. A possible explanation for this discrepancy is that the parameter values estimated for the initial 15 months (Oct. 2013 - Dec. 2014) may not be entirely applicable to the subsequent year (Jan. 2015 - Dec. 2015). This issue might arise from the fact that the biomass data utilized for the inverse model, both in terms of duration and sampling frequency, was insufficient to accurately represent the actual biomass pattern. Consequently, adjusting the time period for model fitting could be necessary to enhance its predictive accuracy. Additionally, the modeled below-ground biomasses for 2015 were generally lower than the field estimates. This discrepancy can be attributed to the fact that field estimates are heavily dependent on measured root:shoot ratios, derived from sediment cores. These measurements are significantly influenced by the heterogeneity in below-ground biomass and may not accurately represent the entire below-ground biomass of a ramet. This issue is evident in the substantial uncertainties observed in some field estimates. Gross et al. (1991) investigated the impact of coring tube size on below-ground biomass estimates in a uniform area of short form S. alterniflora using tubes of varying diameters (3.7 cm to 21.5 cm). Their findings revealed that the smallest diameter cores resulted in the lowest biomass estimates and the highest coefficient of variation (CV), which ranged from 0.59 for a 3.7 cm diameter core to about 0.1 for cores larger than 16.5 cm in diameter. This study suggests the necessity of using cores larger than 16.5 cm to mitigate the effects of below-ground heterogeneity. Our measurements, taken with a 7.5 cm diameter tube, likely provided less representative estimates of true below-ground biomass.

Furthermore, nutrient uptake was not directly incorporated into the model. We applied leaf nitrogen concentrations from tall *S. alterniflora* (Morris et al., 1984) to all height forms. Recent data (1.03 % – 1.99 %) indicating minimal variation in monthly leaf nitrogen content across different height forms of *S. alterniflora* (O'Connell, pers. comm.) contrasts with the wider range (1.25 % – 4 %) reported by Morris et al. (1984). To assess the impact of different nitrogen concentrations on the model, we executed the PG model with double the nitrogen concentration reported by Morris et al. (1984), leading to an approximate doubling in both above- and below-ground biomass estimates. This variation in nitrogen concentration and its effect on model outputs underscores the need for more precise nutrient data.

Accurate field estimates of both above- and below-ground biomass are crucial for parameter determination using the inverse model. This significance is underscored by the tendency of the relatively higher below-ground biomass to dominate the cost function (Eq. 12). Such dominance can lead to less precise estimations of vital above-ground parameters, including translocation and mortality rates. In light of this, we acknowledge advanced modeling techniques that address varying scales of measurement dominating the cost function, such as normalization of variables, and latent-state modeling approaches that evaluate the discrepancy between measured values and unmeasured field data. However, the exploration of these advanced techniques is beyond the scope of our current study. These limitations present opportunities for future research to investigate these sophisticated methods, potentially enhancing the accuracy and applicability of our findings in similar contexts.

5. Conclusion

We have developed a new phenology-based model of the growth and production of above- and below-ground biomass for *S. alterniflora*. The model was parameterized using data collected at the LTER-GCE site on Sapelo Island, Georgia, USA between October 2013 and December 2014, and validated using data from January 2015 through to December 2015. Model results indicate that translocation from below-ground to above-ground tissues may not be essential for survival during the winter months in this region. Our findings suggest a significant contribution to carbon sequestration within the habitat sediment, as evidenced by the substantial mortality rate of below-ground biomass throughout the year. Parameterization of the model also highlights the need for more accurate and precise field estimates of below-ground biomass, especially if hard to measure translocation parameters are to be determined from combining the model with field data. Integrating the salinity effect and computing bidirectional translocation between above- and below-ground tissues during 3 different phenological periods provides new insights into the biomass allocation strategies of this vital blue carbon saltmarsh species.

CRediT authorship contribution statement

Yeajin Jung: Writing – review & editing, Writing – original draft, Visualization, Validation, Software, Investigation, Data curation. **Adrian Burd:** Writing – review & editing, Supervision, Project administration, Investigation, Formal analysis, Conceptualization.

Declaration of Competing Interest

The authors declare that they have no known competing financial interests or personal relationships that could have appeared to influence the work reported in this paper.

Data availability

Data will be made available on request.

Acknowledgements

This work was funded by a National Science Foundation grant (OCE-1237140) and with support from the University of Georgia Graduate School. We would like to thank J. Morris, L. Donovan, M. Alber, and S. Pennings for helpful discussions and the GCE-LTER field crew for their dedication in collecting the samples utilized in this study.

Appendix

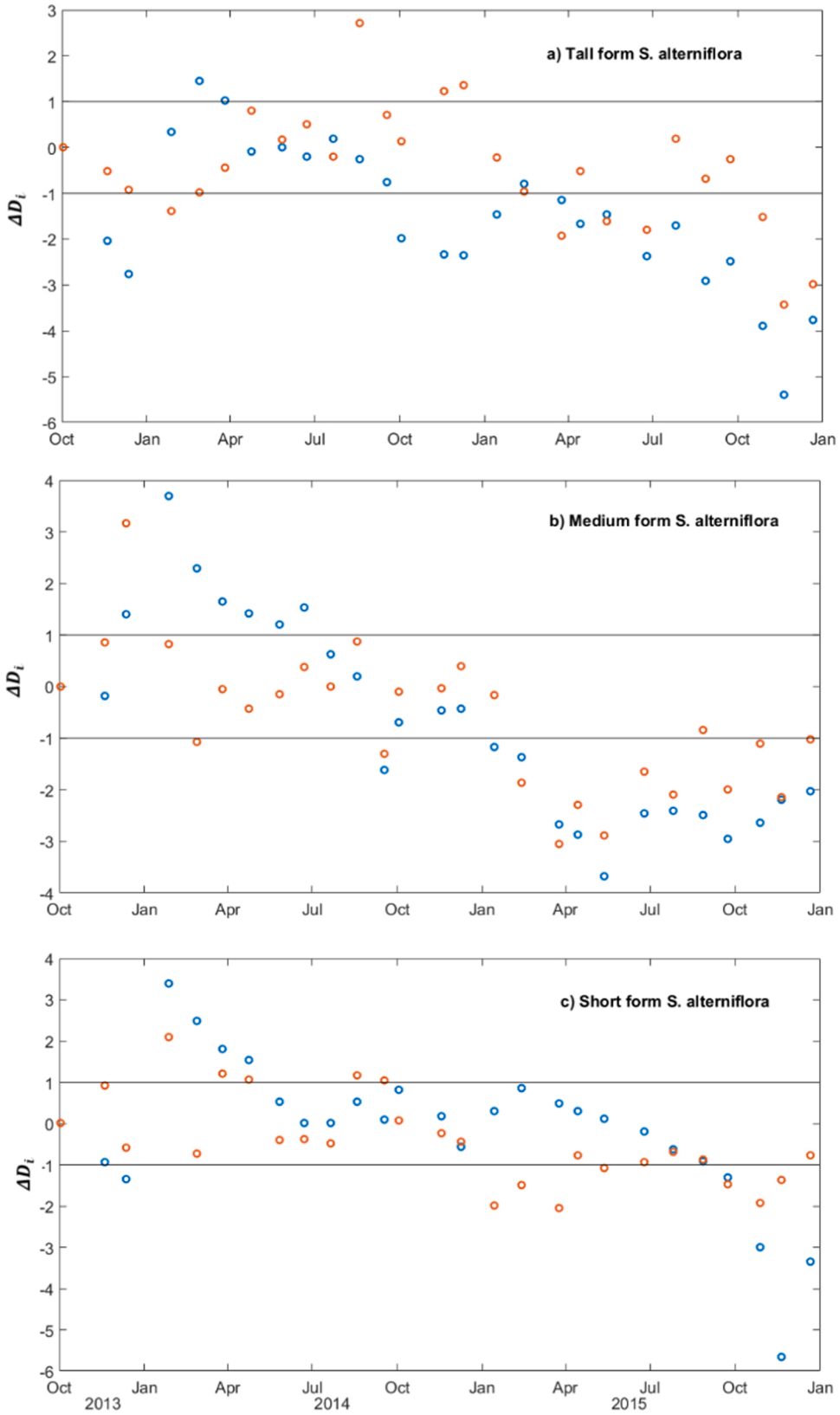

Fig. A.1. ΔD_i values quantifying the differences between observed and modeled biomass in above- (blue circles) and below-ground biomass (red circles) for three height forms of *S. alterniflora*.

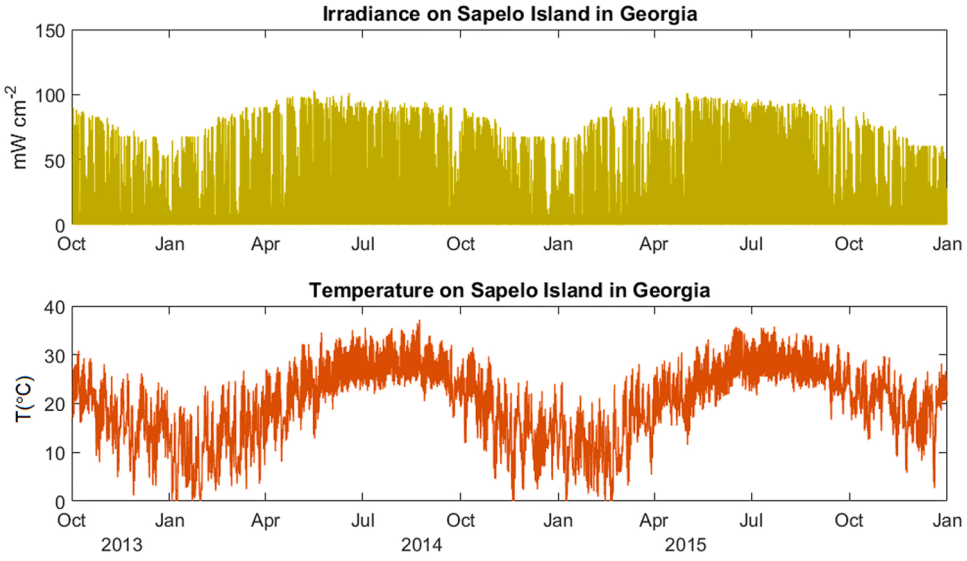

Fig. A.2. Observed downwelling irradiance and temperature on Sapelo Island, Georgia USA.

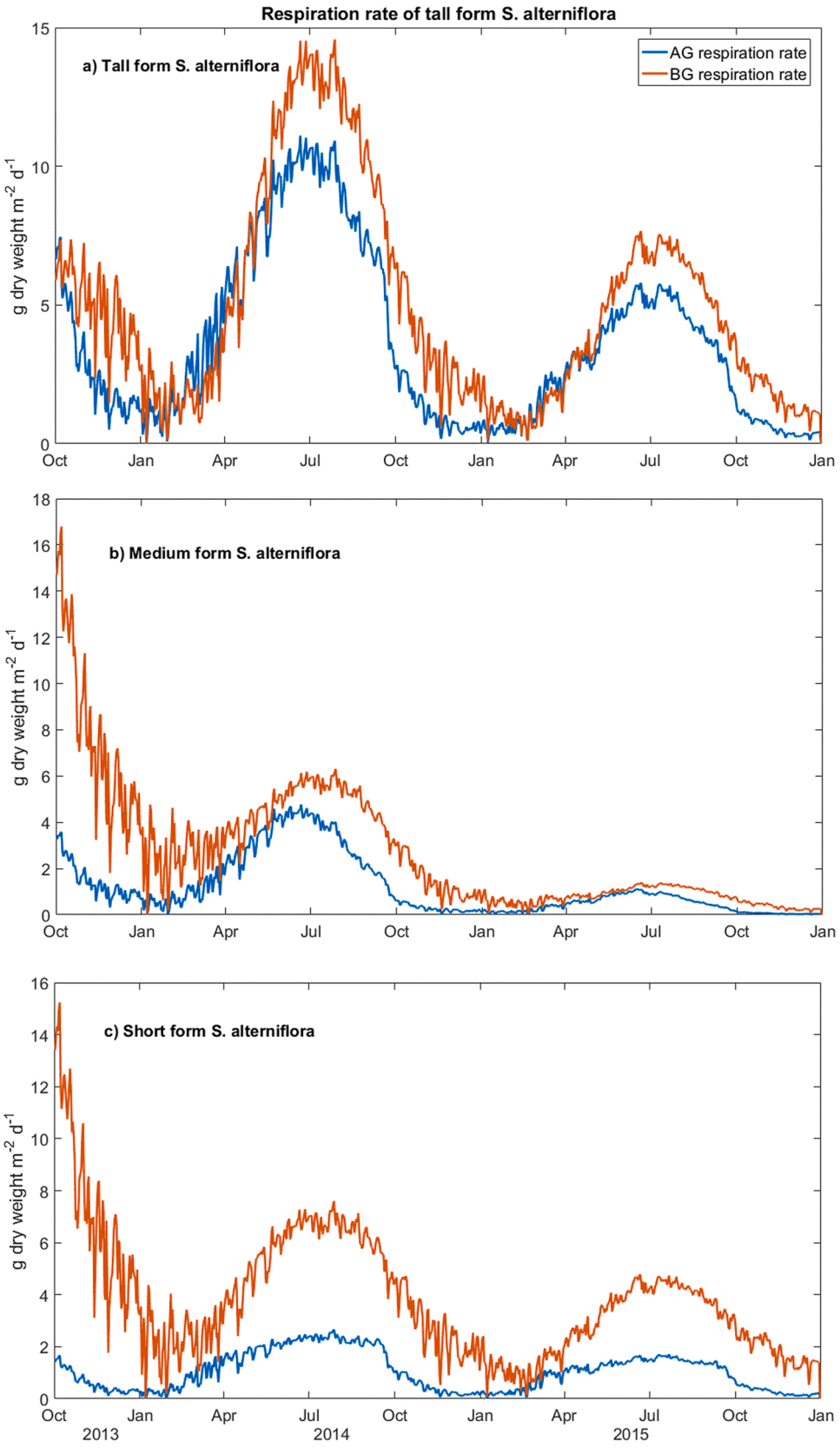

Fig. A.3. Modeled respiration rates of the three types of *S. alterniflora* on Sapelo Island, Georgia.

Table A.1
The monthly average above- and below-ground biomass and the root-to-shoot ratio from two destructive cores

	Tall form *S. alterniflora*			Medium form *S. alterniflora*			Short form *S. alterniflora*		
	Above-ground biomass (g core^{-1})	Below-ground biomass (g core^{-1})	Root to shoot ratio	Above-ground biomass (g core^{-1})	Below-ground biomass (g core^{-1})	Root to shoot ratio	Above-ground biomass (g core^{-1})	Below-ground biomass (g core^{-1})	Root to shoot ratio
Oct−13	35.89	16.51	0.47	8.27	17.87	2.30	2.10	9.30	4.91
Nov−13	24.26	18.84	0.77	9.95	17.09	1.73	5.31	14.86	3.00
Dec−13	19.39	20.92	1.07	10.30	16.15	1.60	1.83	10.69	6.27
Jan−14	8.66	17.48	2.06	1.85	9.33	5.08	0.97	5.25	5.38
Feb−14	1.77	14.92	8.81	1.00	7.65	7.60	0.64	4.77	7.82
Mar−14	5.36	9.39	1.98	2.63	8.10	3.33	1.10	2.90	2.57
Apr−14	12.44	10.00	0.82	2.56	6.48	2.83	1.41	3.83	2.69
May−14	11.64	12.03	1.03	3.85	6.64	1.73	1.75	7.08	4.15
Jun−14	33.21	12.82	0.39	6.38	9.16	1.47	2.36	7.90	3.44
Jul−14	14.65	20.84	1.37	7.51	11.39	1.63	2.46	8.54	3.58
Aug−14	17.37	13.12	0.75	8.84	8.21	1.15	4.04	7.94	1.98
Sep−14	22.64	17.32	0.79	7.83	15.42	2.03	5.80	9.42	1.62
Oct−14	17.74	12.61	0.76	8.19	9.73	1.29	4.45	8.62	2.81
Nov−14	21.21	10.70	0.48	5.11	7.52	1.99	1.43	6.60	4.67
Dec−14	17.66	13.93	0.78	8.42	12.50	1.49	0.98	5.33	6.17
Jan−15	15.11	11.61	0.77	5.86	9.88	1.70	0.54	6.01	11.10
Feb−15	6.07	7.77	1.27	2.78	11.03	4.08	0.70	7.37	10.48
Mar−15	7.06	13.53	1.91	3.00	10.88	3.59	0.81	8.07	10.00
Apr−15	13.97	8.89	0.76	2.15	9.05	4.30	1.14	7.92	7.45
May−15	6.49	11.65	1.78	3.55	13.09	3.77	1.43	7.53	5.23
Jun−15	21.42	20.29	0.96	5.57	9.44	1.87	2.46	11.10	4.46
Jul−15	17.98	9.80	0.53	7.92	12.99	1.66	2.94	9.96	3.25
Aug−15	22.36	13.31	0.86	8.91	10.10	2.29	2.19	9.32	5.11
Sep−15	17.99	9.06	0.52	12.22	17.88	1.60	2.09	9.01	4.61
Oct−15	38.06	19.27	0.56	5.63	12.96	3.42	1.69	10.70	6.35
Nov−15	18.57	13.07	0.72	5.52	17.09	3.12	1.48	10.31	9.58
Dec−15	21.75	17.86	0.81	5.07	13.37	3.20	1.24	7.30	14.50

Table A.2
Biomass translocation across phenological periods in three *S. alterniflora* types (AG: Aboveground, BG: Belowground), The value less than 10^{-7} is denoted as 0.

	Height form	Tall				Medium				Short			
	year	2014	2015	Ave.	% of total TL	2014	2015	Ave.	% of total TL	2014	2015	Ave.	% of total TL
Growing (3/1 ~ 10/ 2)	**Total translocation(TL) from AG to BG** (g dry weight/m^2/period)	5168.3	2713.4	3940.9	93.7 (period)	820.9	186.8	503.9	100	1859.1	1218.2	1538.7	89.3
	Daily translocation (g dry weight/m^2/day)	24.2	12.7	18.4	83.6 (day)	3.8	0.9	2.4	100	8.7	5.7	7.2	74.0

(*continued on next page*)

Table A.2 (*continued*)

	Height form	Tall				Medium				Short			
	year	2014	2015	Ave.	% of total TL	2014	2015	Ave.	% of total TL	2014	2015	Ave.	% of total TL
Senescence (10/2 ~ 12/15)	**Total translocation from AG to BG** (g dry weight/m^2/period)	363.5	165.8	264.6	6.3	0	0	0	0	236.3	131.8	184.0	10.7
	Daily translocation (g dry weight/m^2/day)	5.0	2.3	3.6	16.4	0	0	0	0	3.2	1.8	2.5	26.0
Dormancy (12/15 ~ 2/28)	**Total translocation from BG to AG** (g dry weight/m^2/period)	0	0	0	0	0	0	0	0	0	0	0	0
	Daily translocation (g dry weight/m^2/day)	0	0	0	0	0	0	0	0	0	0		0

Table A.3
Daily mean above- and below-ground mortality and respiration rates (g m^{-2} d^{-1}) estimated in the PG model

	Tall form *S. alterniflora*	Medium form *S. alterniflora*	Short form *S. alterniflora*
Daily mean above-ground mortality rate (g m^{-2} d^{-1})	7.83	4.85	5.78 x 10^{-10}
Daily mean below-ground mortality rate (g m^{-2} d^{-1})	6.82	6.95	2.02
Daily mean above-ground respiration rate (g m^{-2} d^{-1})	3.60	1.17	1.02
Daily mean below-ground respiration rate (g m^{-2} d^{-1})	4.97	2.71	3.82

Table A.4
Sensitivity analysis of phenological dates

(BG_to_AG_START =349) **12/15 (This study)**	Variation (day)	AGB(%)	BGB(%)
	−20	95.98	13.05
	−10	41.48	7.68
	+10	−30.77	−9.34
	+20	−46.17	−17.19
12/10 (O′Connell)	**- 5**	**19.26**	**4.06**
(BG_to_AG_end =59)	Variation	AGB(%)	BGB(%)
2/28 (This study)	(day)		
	−20	0.00	0.00
	−10	0.00	0.00
	+10	0.00	0.00
	+20	0.00	0.00
3/8 (O′Connell)	**+ 8**	**0.00**	**0.00**
(AB_to_BG_START =60)	Variation	AGB(%)	BGB(%)
3/1 (This study)	(day)		
	−20	−20.99	−21.49
	−10	−11.14	−11.44
	+10	25.57	26.54
	+20	55.90	58.55
3/8 (O′Connell)	**+ 7**	**14.17**	**14.65**
(AB_to_BG_END =275)	Variation	AGB(%)	BGB(%)
10/2 (This study)	(day)		
	−20	21.96	15.57
	−10	−0.34	−0.81
	+10	6.03	1.39
	+20	12.53	4.52
9/11 (O′Connell)	**−21**	**26.40**	**18.68**

References

Anderson, C.M., Treshow, M., 1980. A review of environmental and genetic factors that affect height in Spartina alterniflora Loisel.(salt marsh cord grass). Estuaries 3, 168–176.

Asaeda, T., Karunaratne, S., 2000. Dynamic modeling of the growth of *Phragmites australis:* model description. Aquat. Bot. 67 (4), 301–318.

Asaeda, T., Hai, D.N., Manatunge, J., Williams, D., Roberts, J., 2005. Latitudinal characteristics of below- and above-ground biomass of *Typha*: a modelling approach. Ann. Bot. 96 (2), 299–312.

Craft, C., 2023. Tidal marsh restoration on Sapelo Island: A legacy of RJ Reynolds, Jr., Eugene Odum and the University of Georgia Marine Institute. Ecol. Eng. 187, 106875.

Crosby, S.C., Ivens-Duran, M., Bertness, M.D., Davey, E., Deegan, L.A., Leslie, H.M., 2015. Flowering and biomass allocation in U.S. Atlantic coast *Spartina alterniflora*. Am. J. Bot. *102* (5), 669–676. https://doi.org/10.3732/ajb.1400534.

Cunha, S.R.D., Asmus, M.L., & Costa, C.S.B. (2005). Production dynamics of Spartina alterniflora salt marshes in the estuary of Patos Lagoon (RS, Brazil): a simulation model approach.

Dai, T., Wiegert, R.G., 1996. Estimation of the primary productivity of *Spartina alterniflora* using a canopy model. Ecography *19* (4), 410–423.

Davis, J.L., Currin, C.A., O'Brien, C., Raffenburg, C., Davis, A., 2015. Living shorelines: coastal resilience with a blue carbon benefit. PloS One 10 (11), e0142595.

Dawes, C.J., 1998. Marine botany. John Wiley, New York, NY.

Drake, B.G., Gallagher, J.L., 1984. Osmotic potential and turgor maintenance in Spartina alterniflora Loisel. Oecologia 62 (3), 368–375.

Elsey-Quirk, T., Seliskar, D.M., Gallagher, J.L., 2011. Differential population response of allocation, phenology, and tissue chemistry in *Spartina alterniflora*. Plant Ecol. *212* (11), 1873–1885.

Gallagher, J.L., Reimold, R.J., Linthurst, R.A., Pfeiffer, W.J., 1980. Aerial production, mortality, and mineral accumulation-export dynamics in Spartina alterniflora and Juncus roemerianus plant stands in a Georgia salt marsh. Ecology 61 (2), 303–312.

Ge, Z.M., Zhang, L.Q., Yuan, L., Zhang, C., 2014. Effects of salinity on temperature-dependent photosynthetic parameters of a native C3 and a non-native C4 marsh grass in the Yangtze Estuary, China. Photosynthetica *52* (4), 484–492. https://doi.org/10.1007/s11099-014-0055-4.

Geiger, D.R., 1969. Chilling and translocation inhibition. Ohio J. Sci. *69* (6), 356–366.

Gross, M.F., Hardisky, M.A., Wolf, P.L., Klemas, V., 1991. Relationship between aboveground and belowground biomass of *Spartina alterniflora* (smooth cordgrass). Estuaries *14* (2), 180–191.

Hessini, K., Martínez, J.P., Gandour, M., Albouchi, A., Soltani, A., Abdelly, C., 2009. Effect of water stress on growth, osmotic adjustment, cell wall elasticity and water-use efficiency in Spartina alterniflora. Environ. Exp. Bot. 67 (2), 312–319.

Howes, B.L., Dacey, J.W.H., Goehringer, D.D., 1986. Factors controlling the growth form of Spartina alterniflora: feedbacks between above-ground production, sediment oxidation, nitrogen and salinity. J. Ecol. 881–898.

Jung, Y., Burd, A., 2017. Seasonal changes in above- and below-ground non-structural carbohydrates (NSC) in *Spartina alterniflora* in a marsh in Georgia, USA. Aquat. Bot. *140*, 13–22. https://doi.org/10.1016/j.aquabot.2017.04.003.

King, G.M., Klug, M.J., Wiegert, R.G., Chalmers, A.G., 1982. Relation of soil water movement and sulfide concentration to *Spartina alterniflora* production in a Georgia salt marsh. Science *218* (4567), 61–63. https://doi.org/10.1126/science.218.4567.61.

Linthurst, R.A., Seneca, E.D., 1981. Aeration, nitrogen and salinity as determinants of *Spartina alterniflora* Loisel. growth response. Estuaries *4* (1), 53–63.

Mcleod, E., Chmura, G.L., Bouillon, S., Salm, R., Björk, M., Duarte, C.M., Silliman, B.R., 2011. A blueprint for blue carbon: toward an improved understanding of the role of vegetated coastal habitats in sequestering CO2. Front. Ecol. Environ. 9 (10), 552–560.

Medeiros, D.L., White, D.S., Howes, B.L., 2013. Replacement of Phragmites australis by Spartina alterniflora: the role of competition and salinity. Wetlands 33, 421–430.

Miklesh, D., Meile, C., 2018. Porewater salinity in a southeastern United States salt marsh: controls and interannual variation. PeerJ 6, e5911.

Morris, J.T., 1982. A model of growth responses by *Spartina alterniflora* to nitrogen limitation. J. Ecol. *70* (1), 25–42. https://doi.org/10.2307/2259862.

Morris, J.T., Houghton, R.A., Botkin, D.B., 1984. Theoretical limits of belowground production by *Spartina alterniflora*: an analysis through modelling. Ecol. Model. *26* (3), 155–175. https://doi.org/10.1016/0304-3800(84)90068-1.

Nestler, J., 1977. Interstitial salinity as a cause of ecophenic variation in *Spartina alterniflora*. Estuar. Coast. Mar. Sci. *5* (6), 707–714. https://doi.org/10.1016/0302-3524(77)90043-3.

O'Donnell, J.P., Schalles, J.F., 2016. Examination of abiotic drivers and their influence on Spartina alterniflora biomass over a twenty-eight year period using Landsat 5 TM satellite imagery of the Central Georgia Coast. Remote Sens. 8 (6), 477.

Pennings, S.C. (2002). Plant allometry at GCE sampling sites 1-10 in October, 2002. Georgia Coastal Ecosystems LTER Project, University of Georgia, Long Term Ecological Research Network. https://doi.org/10.6073/pasta/e5e854be6597aa4335a2058ffece7fe8.

Peterson, B.J., Howarth, R.W., 1987. Sulfur, carbon, and nitrogen isotopes used to trace organic matter flow in the salt-marsh estuaries of Sapelo Island, Georgia 1. Limnol. Oceanogr. 32 (6), 1195–1213.

Potvin, C., Goeschl, J.D., Strain, B.R., 1984. Effects of temperature and CO_2 enrichment on carbon translocation of plants of the C4 grass species *Echinochloa crus-galli* (L.) Beauv. from cool and warm environments. Plant Physiol. *75* (4), 1054–1057.

Press, W.H., Teukolsky, S.A., Vetterling, W.T., Flannery, B.P., 2002. Numerical Recipies in C++: The Art of Scientific Computing, 2nd ed. Cambridge University Press, Cambridge, UK.

Redfield, A.C., 1972. Development of a New England salt marsh. Ecol. Monogr. *42* (2), 201–237. https://doi.org/10.2307/1942263.

Richards, C.L., Pennings, S.C., Donovan, L.A., 2005. Habitat range and phenotypic variation in salt marsh plants. Plant Ecol. *176* (2), 263–273.

Seneca, E.D., Blum, U., 1984. Response to photoperiod and temperature by *Spartina alterniflora* (Poaceae) from North Carolina and *Spartina folisa* from California. Am. J. Bot. *71* (1), 91–99. https://doi.org/10.2307/2443628.

Seneca, E.D., Broome, S.W., 1972. Seedling response to photoperiod and temperature by smooth cordgrass, *Spartina alterniflora*, from Oregon Inlet, North Carolina. Chesap. Sci. *13* (3), 212–215. https://doi.org/10.2307/1351066.

Shepard, C.C., Crain, C.M., Beck, M.W., 2011. The protective role of coastal marshes: a systematic review and meta-analysis. PloS One 6 (11), e27374.

Smart, M.L. (1986). *Intraspecific competition and growth form differentiation of the salt marsh plant, Spartina alterniflora Loisel* (Doctoral dissertation), University of Delaware, Newark, DE.

Soetaert, K., Petzoldt, T., 2010. Inverse modelling, sensitivity and Monte Carlo analysis in R using package FME. J. Stat. Softw. 33, 1–28.

Stagg, C.L., Schoolmaster Jr, D.R., Piazza, S.C., Snedden, G., Steyer, G.D., Fischenich, C. J., McComas, R.W., 2017. A landscape-scale assessment of above- and belowground primary production in coastal wetlands: Implications for climate change-induced community shifts. Estuaries Coasts *40* (3), 856–879. https://doi.org/10.1007/s12237-016-0177-y.

Townend, I., Fletcher, C., Knappen, M., Rossington, K., 2011. A review of salt marsh dynamics. Water Environ. J. 25 (4), 477–488.

Więski, K., Pennings, S.C., 2014. Climate drivers of Spartina alterniflora saltmarsh production in Georgia, USA. Ecosystems 17, 473–484.

Whitfield, A.K., 2017. The role of seagrass meadows, mangrove forests, salt marshes and reed beds as nursery areas and food sources for fishes in estuaries. Rev. Fish. Biol. Fish. 27 (1), 75–110.

Zheng, S., Shao, D., Asaeda, T., Sun, T., Luo, S., Cheng, M., 2016. Modeling the growth dynamics of *Spartina alterniflora* and the effects of its control measures. Ecol. Eng. *97*, 144–156. https://doi.org/10.1016/j.ecoleng.2016.09.006.